THE JOURNAL OF PHYSICAL CHEMISTRY B

Article

Cite This: J. Phys. Chem. B 2018, 122, 10097−10107

pubs.acs.org/JPCB

Influence of the Electrochemical Properties of the Bacteriochlorophyll Dimer on Triplet Energy-Transfer Dynamics in Bacterial Reaction Centers

Sarthak Mandal,*[,†,§] Eduardo Espiritu,[‡] Natalie Akram,[†] Su Lin,[†,‡] JoAnn C. Williams,[‡] James P. Allen,[‡] and Neal W. Woodbury*[,†,‡]

[†]Center for Innovations in Medicine, The Biodesign Institute and [‡]School of Molecular Sciences, Arizona State University, Tempe, Arizona 85281, United States

Supporting Information

ABSTRACT: Energetics, protein dynamics, and electronic coupling are the key factors in controlling both electron and energy transfer in photosynthetic bacterial reaction centers (RCs). Here, we examine the rates and mechanistic pathways of the $P^+H_A^-$ radical-pair charge recombination, triplet state formation, and subsequent triplet energy transfer from the triplet state of the bacteriochlorophyll dimer (P) to the carotenoid in a series of mutant RCs (L131LH + M160LH (D1), L131LH + M197FH (D2), and L131LH + M160LH + M197FH (T1)) of *Rhodobacter sphaeroides*. In these mutants, the electronic structure of P is perturbed and the P/P^+ midpoint potential is systematically increased due to addition of hydrogen bonds between P and the introduced residues. High-resolution, broad-band, transient absorption spectroscopy on the femtosecond to microsecond timescale shows that the charge recombination rate increases and the triplet energy transfer rate decreases in these mutants relative to the wild type (WT). The increase of the charge recombination rate is correlated to the increase in the energy level of $P^+H_A^-$ and the increase in the P/P^+ midpoint potential. On the other hand, the decrease in rate of triplet energy transfer in the mutants can be explained in terms of a lower energy of ^3P and a shift in the electron spin density distribution in the bacteriochlorophylls of P. The triplet energy-transfer rate follows the order of WT > L131LH + M197FH > L131LH + M160LH > L131LH + M160LH + M197FH, both at room temperature and at 77 K. A pronounced temperature dependence of the rate is observed for all of the RC samples. The activation energy associated to this process is increased in the mutants relative to WT, consistent with a lower ^3P energy due to the addition of hydrogen bonds between P and the introduced residues.

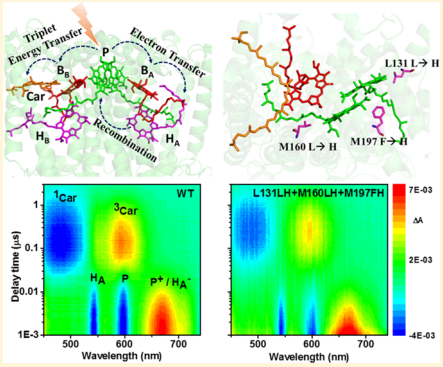

1. INTRODUCTION

Proper photoprotection is critical for maximizing productivity in photosynthetic organisms.[1,2] Various photoprotective mechanisms are employed to prevent the generation of reactive oxygen species under excess illumination.[3−6] Carotenoids play a key role in these photoprotective processes, in addition to their importance in light harvesting.[5,7] In the light-harvesting (LH) complexes of higher plants, photoprotection is achieved by dissipating excess excitation energy of chlorophylls via pathways, including triplet energy transfer to the carotenoid[6] and nonphotochemical quenching of chlorophyll fluorescence, through interactions with carotenoid.[3] In photosynthetic bacterial reaction centers (RCs), the triplet state of the primary donor, P (a bacteriochlorophyll dimer), can be generated upon excess illumination and is quenched by triplet energy transfer to the carotenoid (Car).[8−14]

In RCs, there are a series of co-factors involved in energy and electron transfer, including the primary donor (P), two bacteriochlorophyll monomers (B_A and B_B), two bacteriopheophytins (H_A and H_B), two quinones (Q_A and Q_B), a carotenoid, and a nonheme iron. With the exception of the carotenoid, these co-factors are arranged in two quasi-symmetrical chains known as the A and B chains. Electron transfer occurs exclusively through the A chain under normal conditions (Figure 1a).[15,16] The asymmetric carotenoid molecule is present in the B chain in van der Waals contact with B_B.[15,17] The charge-separated radical pair, $^1(P^+H_A^-)$, is formed in 2−3 ps upon photoexcitation of P in wild-type (WT) RCs.[18−20] When H_A^- to Q_A electron transfer (occurring in a 200 ps timescale) is blocked, $^1(P^+H_A^-)$ can either recombine to the ground state or undergo a singlet−triplet spin dephasing process to form the triplet state of the radical pair, $^3(P^+H_A^-)$, through hyperfine interactions.[21−23] The triplet radical pair then recombines to generate ^3P (see kinetic scheme in Figure 1b).[22,23]

Received: August 16, 2018
Revised: October 8, 2018
Published: October 11, 2018

DOI: 10.1021/acs.jpcb.8b07985
J. Phys. Chem. B 2018, 122, 10097−10107

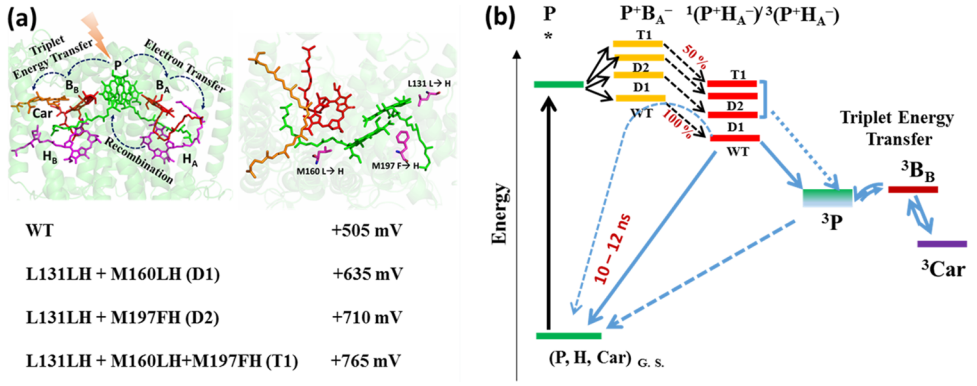

Figure 1. (a) Arrangement of the co-factors in reaction centers and the pathways of electron transfer, charge recombination, and triplet energy transfer between the co-factors (left side). The relative positions of the point mutations that introduce hydrogen bonds between the amino acid residues and P are shown (right side). The increase in the P/P^+ midpoint potential of the mutant reaction centers with increasing the number of hydrogen bonds between P and amino acid residues is shown below the structures. (b) The relative energetics of charge-separated states increases with increasing the P/P^+ midpoint potential causing a decrease in the rate and yield of charge separation ($P^* \rightarrow P^+B_A^- \rightarrow P^+H_A^-$ in quinone-depleted RCs). The kinetic pathway of triplet P formation and subsequent triplet energy transfer is also shown.

The ^3P generated is efficiently (nearly 100% in WT RCs) quenched by the carotenoid (here, sphaeroidenone in 15,15′-cis conformation), which has a lower triplet state energy than ^3P.[24,25] This quenching prevents the interaction of ^3P with oxygen and the generation of reactive oxygen species. The triplet energy transfer is thought to occur via a Dexter mechanism requiring relatively strong electronic orbital overlap.[26,27] A bacteriochlorophyll, B_B, is located between P and carotenoid[24,25,28] and is presumably involved as an intermediate in the triplet energy transfer. However, there is no direct evidence for participation of ^3B_B during the process. The rates and mechanistic pathways of $^3P \rightarrow {}^3B_B \rightarrow {}^3Car$ triplet energy transfer in WT and B_B co-factor-modified mutant RCs have been studied previously using transient absorption, time-resolved electron paramagnetic resonance (EPR), and other spectroscopic techniques.[10,14,29−32] This work has implied that the triplet energy transfer occurs through a thermally activated mechanism, where the intermediate state, ^3B_B, is nearly 100 cm^{-1} higher in energy than triplet state of ^3P in WT.[12,14,29] Recently, we have explored the details of the triplet energy transfer mechanism in WT and the Φ mutant, M182HL RC, where B_B is replaced by a bacteriopheophytin, using high-resolution broad-band transient absorption spectroscopy.[14] From the spectral and kinetic analyses, it was shown that B_B has substantial electronic coupling to both ^3Car and ^3P and that this likely mediates the rapid and efficient triplet energy transfer observed in WT. In the Φ mutant, the triplet energy of the bridging intermediate is increased by replacement of the co-factor B_B by a bacteriopheophytin, and the reaction rate decreased significantly, consistent with the idea that ^3B_B acts as a thermally activated bridging state (triplet bacteriopheophytin is expected to be at higher energy than the triplet monomer bacteriochlorophyll normally present in the B_B pocket); no triplet energy transfer was observed at low temperature (77 K) in the Φ mutant.

Previous work has primarily focused on the mechanistic implications of changing the energetics of either ^3B_B or ^3Car via mutation or substitution, and the effects of perturbing these energies are reasonably well understood.[10,11,24,28,30,33] However, perturbation of the electronic structure and triplet energetics of P on triplet energy transfer has not been systematically explored. The electronic spin density on P is asymmetrically distributed between the two bacteriochlorophylls, as shown earlier by EPR and ENDOR studies.[34] This asymmetric spin density distribution may also affect the triplet state delocalization of P and the electronic coupling between ^3P and the monomeric bacteriochlorophylls of RCs.[35]

In this work, a systematic study of the rates and kinetic pathways of charge recombination, triplet state formation, and triplet energy transfer in WT and in a series of three different RC mutants of *Rhodobacter sphaeroides* (L131LH + M160LH (D1), L131LH + M197FH (D2), and L131LH + M160LH + M197FH (T1)) is presented. These double (D1 and D2) and triple (T1) mutants introduce new hydrogen bonds with P,[36,37] altering its electronic spin distribution and raising the P/P^+ midpoint potential from 505 mV in WT to 635, 710, and 765 mV in the D1, D2, and T1 mutant RCs, respectively (Figure 1a).[38,39] The energetics of the charge-separated states ($P^+B_A^-$, $P^+H_A^-$, etc.) relative to the ground states of P, B, and H (Figure 1b) increases with increasing P/P^+ midpoint potential,[19] and these mutants have been useful in studying the rate vs driving force dependence of charge separation and recombination processes.[19,40] The spin density distribution of the bacteriochlorophylls in P also changes when hydrogen bonds are added to P in the mutant RCs.[41−43] Here, the triplet state formation and triplet energy transfer processes in the D1, D2, and T1 mutant RCs are explored and compared to the results in WT RCs. First, the effect of systematically altering the energetics of the $P^+H_A^-$ radical-pair charge-separated state on the rate and yield of ^3P formation is measured. ^3P is formed during the decay of $^3(P^+H_A^-)$, and the competition between singlet radical-pair recombination and singlet−triplet spin dephasing determines the yield of ^3P. The temperature-dependent rates and pathways for the decay of ^3P (either by triplet energy transfer or by direct decay to the ground state of P) are then compared between the WT and mutant RCs, focusing on the effects of changes in the spin density distribution and the triplet state energetics induced by the mutations.

2. MATERIALS AND METHODS

The construction, isolation, and purification of the mutants, L131LH + M160LH (D1), L131LH + M197FH (D2), L131LH + M160LH + M197FH (T1), and the carotenoid-

DOI: 10.1021/acs.jpcb.8b07985
J. Phys. Chem. B 2018, 122, 10097−10107

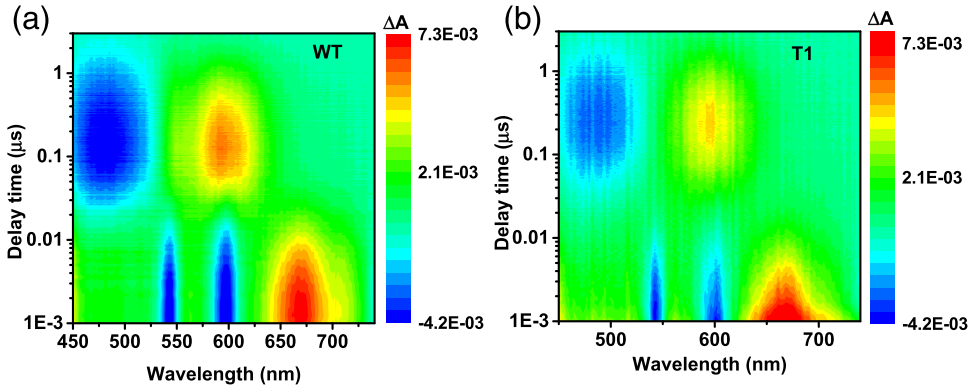

Figure 2. Contour plots of transient absorption changes in the Q_X absorption region of (a) quinone-depleted WT and (b) quinone-depleted L131LH + M160LH + M197FH (T1) mutant RCs recorded at room temperature after excitation at 865 nm.

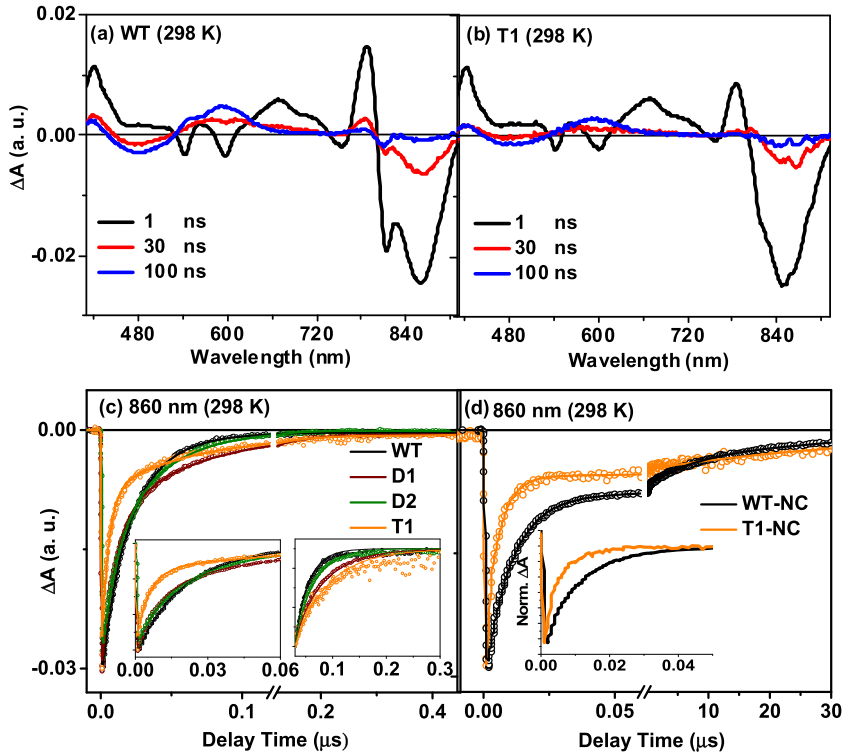

Figure 3. (a, b) Time-resolved absorption difference spectra of quinone-depleted WT and L131LH + M160LH + M197FH (T1) mutant RCs at 1, 30, and 100 ns time delays recorded at room temperature after excitation at 865 nm. (c) Kinetic traces of the WT, L131LH + M160LH (D1), L131LH + M197FH (D2), and T1 RCs monitored at 860 nm showing the recovery of P bleaching during the radical-pair charge recombination, ^{3}P formation and subsequent triplet energy-transfer processes. Inset: the left panel shows the kinetics (1−50 ns) dominated by charge recombination (traces are normalized to the same initial amount of P bleaching at 1 ns) and the right panel shows the kinetic traces (normalized to the same amount of P bleaching corresponding to ^{3}P population at 30 ns) in the time region 30−300 ns dominated by triplet energy transfer. (d) The kinetic traces of WT-NC and T1-NC reaction centers monitored at 860 nm showing the recovery of the P bleaching due to radical-pair charge recombination and the direct decay of ^{3}P to the ground-state P.

less mutants, M71GL (WT-NC) and L131LH + M160LH + M197FH + M71GL (T1-NC), have been described previously.[39,44] To block electron transfer to Q_A and generate ^{3}P, both Q_A and Q_B were removed from the RCs[14,45] (90−95% removal of Q_A as measured by light-minus-dark spectroscopy). The quinone-depleted RCs were suspended in 15 mM Tris−HCl (pH 8.0) buffer containing 0.045% lauryl dimethylamine oxide, 1 mM ethylenediaminetetraacetic acid, and 150 mM NaCl. For transient absorption measurements, the RC samples were loaded into a 2 mm cuvette with a final absorbance at 800 nm of ∼0.8. For low-temperature measurements, the RC samples were dissolved in 3:1 (v/v) glycerol−buffer mixture.[14]

A detailed description of the ultrafast pump-probe absorption spectroscopy setup has been reported previously.[18] Briefly, a regenerative optical amplifier (consisting of a Tsunami Oscillator and a Spitfire amplifier, Spectra-Physics) was used to generate 1 mJ laser pulses at a repetition rate of 1 kHz (100 fs pulse duration, 800 nm). Part of the pulse energy (600 μJ) was used to pump an optical parametric amplifier (OPA-800, Spectra-Physics) to generate the excitation pulses at 865 nm for room-temperature measurements and at 870 nm for measurements at 77 K. The broad-band transient

DOI: 10.1021/acs.jpcb.8b07985
J. Phys. Chem. B 2018, 122, 10097−10107

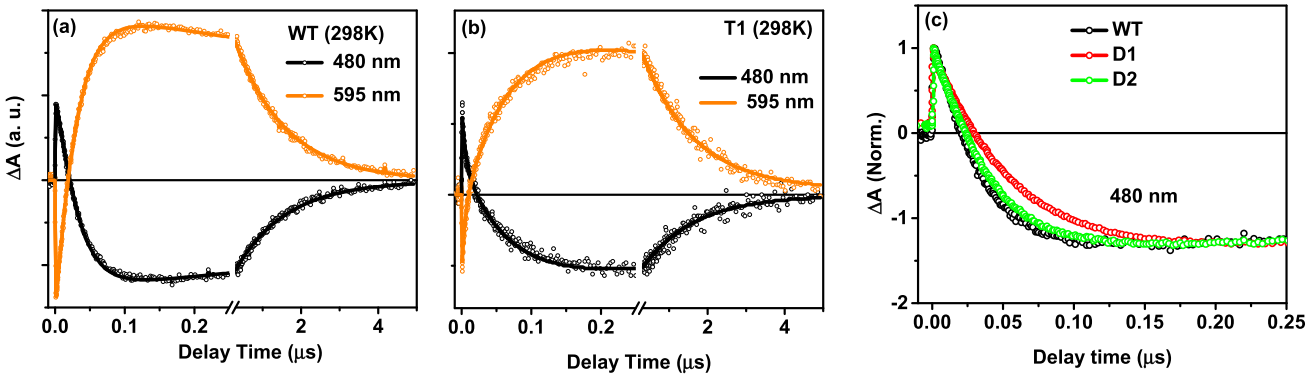

Figure 4. Kinetic traces of carotenoid ground-state bleaching and the ^{3}Car absorption increase monitored at 480 and 600 nm, respectively, for RCs from (a) WT and (b) the triple mutant (T1, L131LH + M160LH + M197FH). (c) Comparison of the evolution of the kinetics of the carotenoid bleaching signal (at 480 nm) between RCs from WT, (L131LH + M160LH) and (L131LH + M197FH).

absorption changes were measured using a spectrophotometer that included a charge-coupled device as a detector (DU420, Andor Technology). The polarization of the pump pulses was set to the magic angle (54.7°) with respect to the probe pulse polarization. Transient spectra were recorded between 500 and 760 nm at delay times from 100 fs to 7 ns.

For transient absorption measurements in the nanosecond to microsecond time region, a commercial spectrometer (EOS VIS−NIR, Ultrafast Systems, Sarasota, FL) was used. This system has a broad-band probe light that covers the entire wavelength region from 400 to 910 nm.[14,46] The pump pulse was generated from the same ultrafast laser system, as discussed above.

3. RESULTS AND DISCUSSION

3.1. Ground-State Absorption Spectra. The ground-state absorption spectra of all of the mutant RCs, D1, D2, T1, WT-NC, and T1-NC, are compared with WT RCs in Figure S1. The mutants have spectra similar to WT, consistent with prior studies.[38] Thus, the energy of the singlet-excited state of P does not change as a result of the mutations. In mutants WT-NC and T1-NC, the carotenoid is not present due to the change of glycine to leucine at M71 (M71GL) and as a result a significantly reduced absorption is observed in the 450−550 nm region (sphaeroidenone under the growth conditions used).[44] The absence of the carotenoid in these mutants also causes a slight blue shift of the Q_Y absorption of B_A/B_B (at 800 nm) compared to WT (at 802 nm).[17]

3.2. Nanosecond Transient Absorption Data at Room Temperature. The dynamics of $P^+H_A^-$ charge recombination, triplet state formation, and triplet energy transfer in the quinone-depleted WT and mutant RCs were monitored using transient absorption spectroscopy in the spectral range 410−910 nm with a time resolution of 1 ns. The two-dimensional pseudocolor contour plots for WT and the mutant T1 between 450 and 740 nm (the Q_X absorption region) are shown in Figure 2. The corresponding plots for the other mutants (D1, D2, WT-NC, and T1-NC) are shown in Figure S2. Initially (within 1 ns), following photoexcitation, the accumulation of $^1(P^+H_A^-)/^3(P^+H_A^-)$ results in the appearance of negative bands at 545 and 600 nm corresponding to a decrease in ground-state absorbance for H_A and P, respectively. There are also positive bands at 665 and 700 nm that correspond to the absorbance of P^+ and H_A^-, respectively. These bands largely disappear as $^1(P^+H_A^-)/^3(P^+H_A^-)$ decays and ^{3}P appears. Triplet energy transfer from ^{3}P to the carotenoid results in the appearance of the ^{3}Car absorption band at 600 nm and a decrease in the ground-state carotenoid band at 480 nm. The Car ground-state absorbance decrease and the ^{3}Car absorption increase are absent in the WT-NC and T1-NC mutants consistent with the absence of triplet energy transfer in these carotenoid-less RCs (Figure S2c,d). The data for WT RCs are consistent with the previously reported data.[14]

The differences between the spectral evolution of WT and D1, D2 and T1 mutants can be better understood by considering spectra at several characteristic delays (1, 30, and 100 ns) from the data (see Figures 3a,b and S3). At 1 ns, reaction centers are predominantly in the $^1(P^+H_A^-)/^3(P^+H_A^-)$ state, and there is prominent loss of ground-state absorbance at 860 and 600 nm (P), 760 and 545 nm (H_A) as well as broad absorption increases between 660 and 700 nm due to the absorption by H_A^- and P^+.[14] These absorbance changes largely disappear by 30 ns due to the decay of $^1(P^+H_A^-)/^3(P^+H_A^-)$.[47,48]

What remains of the ground-state bleaching of P at 30 ns is largely due to ^{3}P. By 100 ns, ^{3}P has almost completely decayed via triplet energy transfer to the carotenoid.[25,29] The 100 ns spectrum of the carotenoid-containing RCs shows carotenoid ground-state bleaching between 450 and 550 nm as well as ^{3}Car absorption at 600 nm as expected for the ^{3}Car state.[11,25,28] The ^{3}Car decays by 3 μs at room temperature for all of the carotenoid-containing RC samples (Figure S4). As expected, in the WT-NC and T1-NC mutants, the spectra lack characteristics of ^{3}Car formation (Figure S5).[14] The ^{3}P population (residual P bleaching in 30 ns spectra) in these carotenoid-less RCs decays by 30 μs (Figure S5).

A comparison of the P bleaching amplitudes in the 30 ns spectra between WT and the mutants shows a significantly lower yield of ^{3}P in the T1 mutant (Figure S6a). However, no significant difference in the yield of ^{3}P is observed between the WT and double mutants D1 and D2 (the relative amplitude of P bleaching in the 30 ns spectra is similar for WT, D1, and D2 in Figure S6a). The poor yield of ^{3}P in the T1 mutant compared to WT is also reflected in a comparison of the 30 ns spectra of the WT-NC and T1-NC (Figure S6b). In these comparisons, the spectra were scaled in such a way that the initially populated $^1(P^+H_A^-)$ state at 1 ns delay time is similar for all RCs.[49] Because of the poor yield of ^{3}P in the T1 mutant, the yield of ^{3}Car also becomes much lower in the carotenoid-containing version of the T1 mutant than in WT, D1, or D2

DOI: 10.1021/acs.jpcb.8b07985
J. Phys. Chem. B 2018, 122, 10097−10107

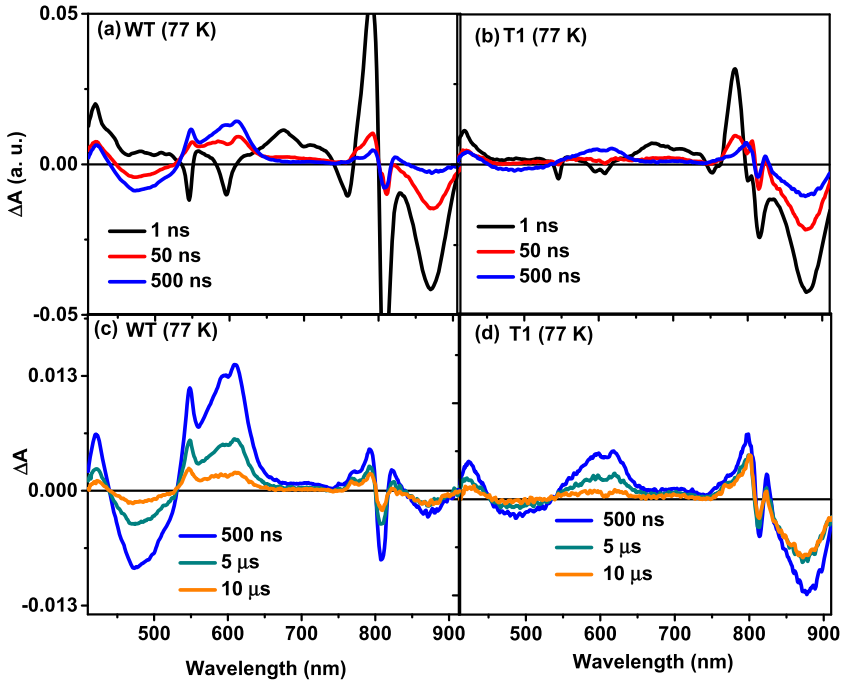

Figure 5. Time-resolved absorption difference spectra of quinone-depleted WT (a, c) and quinone-depleted T1 triple mutant, L131LH + M160LH M197FH (b, d) reaction centers at 77 K. The spectra are recorded at several time delays in the nanosecond to microsecond range after the excitation of samples at 880 nm.

mutants containing carotenoid (see the comparison of the amplitudes of the carotenoid bleaching band at 450−550 nm and ^{3}Car absorption band at 600 nm in the 100 ns spectrum, Figure S6c).

Figure 3c,d shows the P bleaching decay traces at 860 nm for all of the RC samples. Initial 1−30 ns traces suggest a faster $^1(P^+H_A^-)/^3(P^+H_A^-)$ recombination process for the D1, D2, and T1 mutants than WT (inset, left panel of Figure 3c). The residual signal (at 30 ns), which represents the ^{3}P population, decays completely to zero within 100−200 ns for the carotenoid-containing RCs. However, in WT-NC and T1-NC, the ^{3}P signal decays almost 2 orders of magnitude more slowly (20−30 μs) due to the absence of triplet energy transfer (Figure 3d). This supports a nearly 100% yield of triplet energy transfer from ^{3}P to the carotenoid in the carotenoid-containing WT and mutants at room temperature. The evolution and decay kinetic traces of carotenoid ground-state bleaching (at 480 nm) and ^{3}Car absorption (at 595 nm) show clear differences in the dynamics of triplet energy transfer between WT and the mutants (D1, D2, and T1) (Figure 4), which is consistent with that observed from the decay kinetics of the ground-state bleaching of P in Figure 3c.

3.3. Nanosecond Transient Absorption Data at 77 K.

As studied previously, the ^{3}P → ^{3}Car energy transfer in WT RCs is strongly dependent on temperature.[14] The low-temperature (77 K) transient absorption spectra of the WT, D1, D2, and T1 mutant RCs at several characteristic time delays in the nanosecond (1, 50, and 500 ns) to microsecond (5 and 10 μs) region are compared (Figures 5 and S7). The spectral features of the WT are consistent with previously reported low-temperature spectra.[14] At 77 K, the $^1(P^+H_A^-)/^3(P^+H_A^-)$ population observed at 1 ns decays completely by 50 ns for both the WT and mutant samples, judging from the recovery of the H_A ground-state absorbance at 545 nm. The 50 ns spectrum contain prominent P bleaching at 870 nm primarily due to ^{3}P. However, some ^{3}Car is evident as carotenoid ground-state bleaching at 480−500 nm and ^{3}Car absorption increase at 600 nm. This is obvious in the 50 ns spectrum of WT.[14] In the 50−500 ns time range, the P ground-state bleaching at 870 nm (due to the ^{3}P) gradually recovers due to triplet energy transfer at 77 K.

For the carotenoid-containing WT and the D2 mutants, the ^{3}P decays almost to zero by 500 ns (Figures 5a,c and S7a,c). Note that the small residual absorbance decreases, which are associated to B_B (at 800−812 nm) and P (At 870 nm) in the 500 ns and microsecond spectra, are due to the effects of ^{3}Car on the P and B_B ground-state transitions.[14] In contrast, the 500 ns transient absorption spectra of the carotenoid-containing T1 and D1 mutant (Figures 5d and S7d) have a significant amount of actual P ground-state bleaching (at 870 nm) due to residual ^{3}P. For D1, this residual ^{3}P decays with the same kinetics as ^{3}Car (on the 5 μs timescale) (Figure S7d). However, in T1, the residual ^{3}P (present at 500 ns) decays partly in correlation with the decay of ^{3}Car, and the rest decays directly to the ground-state P (in the 100−200 μs time range) without involving triplet energy transfer (Figure 5d). This is consistent with heterogeneous kinetics of triplet energy transfer in D1 and T1 mutants.

In the low-temperature spectra of the carotenoid-less mutants (WT-NC and T1-NC), there is essentially no decay of ^{3}P (residual signal at 50 ns) in the 50−500 ns time range. The ^{3}P in these RCs decays to the ground state more slowly on the 100−200 μs timescale due to the absence of triplet energy transfer (Figure S8). This is consistent with a near 100% efficient triplet energy transfer for WT, D1, and D2 at 77 K, similar to that observed at 298 K. However, for T1, the efficiency is reduced as some population of ^{3}P directly decay to the ground state.

The kinetics of P ground-state bleaching recovery monitored at 870 nm (Figure 6a) were compared between the WT and

DOI: 10.1021/acs.jpcb.8b07985
J. Phys. Chem. B 2018, 122, 10097−10107

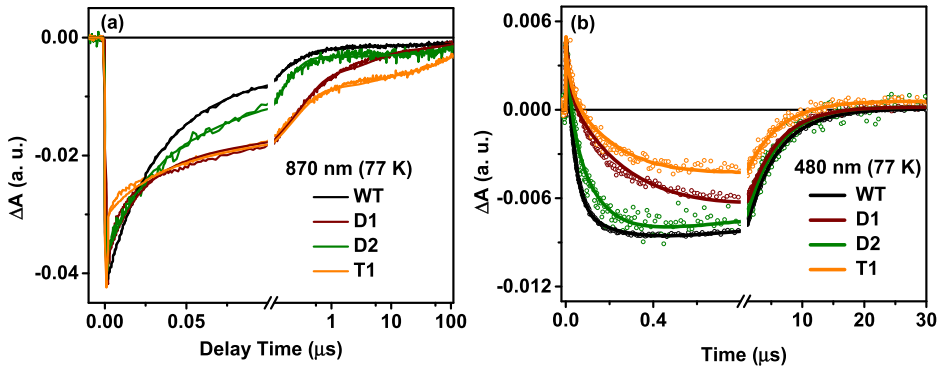

Figure 6. Kinetic traces of quinone-depleted RCs from WT as well as the L131LH + M160LH (D1), L131LH + M197FH (D2), and L131LH + M160LH + M197FH (T1) mutants monitored at 77 K. (a) Absorbance changes at 870 nm showing the recovery of P ground-state bleaching due to either singlet radical-pair charge recombination or energy transfer depleting ^{3}P formation. (b) Absorbance changes at 480 nm showing the formation and decay of ground-state bleaching due to ^{3}Car.

mutant RCs at 77 K. The initial bleaching recovery for the T1 mutant has a rapid phase on the 1−2 ns time range. This fast decay arises from the decay of some P* to ground-state P. The intrinsic lifetime of P* in the absence of electron transfer is in the range of 150−200 ps for WT RCs at room temperature.[20] Nagarajan et al.[50] earlier reported that for the M210YF mutant RCs, where the free-energy gap between $P^+B_A^-$ and $P^+H_A^-$ is increased by the mutation, the intrinsic lifetime of P* became more than 300 ps at room temperature and in the nanosecond range at low temperature. Rapid recovery of P bleaching in the 1−2 ns time is also observed for the T1-NC mutant (Figure S9a). However, the H_A bleaching recovery time in the T1-NC mutant at 545 nm (Figure S9b) is essentially identical to WT-NC, suggesting that at 77 K the decay kinetic traces of $^1(P^+H_A^-)/^3(P^+H_A^-)$ are similar for all of the RC samples irrespective of the P/P^+ midpoint potential. This is consistent with the previous reports, which suggested that the slow component of the $^1(P^+H_A^-)/^3(P^+H_A^-)$ decay is independent of the P/P^+ midpoint potential.[51]

There are significant differences in the P ground-state bleaching recovery traces of the WT, D1, D2, and T1 mutants (Figure 6a) beyond 50 ns at 77 K. The decay traces in this time region, which primarily represent the decay of ^{3}P by triplet energy transfer, become slower in the mutants than in WT following the order of WT (fastest) > D2 > D1 > T1 (slowest). This trend is similar to that observed at room temperature. The kinetic traces of carotenoid ground-state bleaching at 480 nm (Figure 6b) show differences in the rate and yield of ^{3}Car formation for these samples that are consistent with ^{3}P decay (Figure 6a).

3.4. Global Fitting Analysis and the Evolution-Associated Difference Spectra (EADS). Global fitting analysis of the full transient absorption data was performed using a sequential kinetic model [A → B → ···] for all of the samples at room temperature and at 77 K. A three-step kinetic model adequately fits the data sets of the carotenoid-containing RCs, except the low-temperature (77 K) data of T1, which required an additional component for satisfactory fitting. Figures S10 and S11 show the obtained EADS and lifetime components associated to the dynamics (nanosecond to microsecond time) of the carotenoid-containing RCs (WT, D1, D2, and T1 RCs) at room temperature and low temperature, respectively (Table S1). On the basis of the spectral signature (as described in the analysis of the time-resolved spectra), the three EADS are attributed to the decay of $^1(P^+H_A^-)/^3(P^+H_A^-)$, the ^{3}P to ^{3}Car triplet energy transfer, and the decay of ^{3}Car. The additional fourth component (longest 110-μs EADS) obtained for the T1 mutant at 77 K can be attributed to the direct decay of ^{3}P to the ground-state P (Figure S11d).[14,29]

As seen in Figure S10a, the first EADS representing $^1(P^+H_A^-)/^3(P^+H_A^-)$ has a decay time of 12 ns in WT consistent with a previous report.[14] The decay time decreases to 10 ns in D1 and D2 mutants and 5 ns in T1 mutant (Figure S10b−d). This decrease of the $^1(P^+H_A^-)/^3(P^+H_A^-)$ decay time (or the increase of the recombination reaction rate) is consistent with the increase of P/P^+ midpoint potential of the mutant RCs.[19]

As the temperature is lowered, the decay time of $^1(P^+H_A^-)/^3(P^+H_A^-)$ is known to increase for the WT RC, primarily due to the slowing of $^1(P^+H_A^-) \rightarrow (P, H)_{g.s}$ singlet recombination reaction.[14] At very low temperature (77 K), the $^1(P^+H_A^-)/^3(P^+H_A^-)$ state has a similar decay time in the range of 17−22 ns for all samples (Figure S11), suggesting a negligible influence of the P/P^+ midpoint potential on the slower phase of the decay (Table S1) consistent with the previous reports.[19,51]

The decay of $^1(P^+H_A^-)/^3(P^+H_A^-)$ results in the accumulation of ^{3}P as evidenced in the second EADS with prominent P bleaching (860 nm at room temperature and 870 nm at 77 K) and complete recovery of the H_A bleaching (at 545 nm). On the basis of the residual P bleaching signal in these EADS, the yield of ^{3}P was estimated and is presented in Table S1. At room temperature, the ^{3}P state decays by triplet energy transfer with lifetime components of 25, 55, 36, and 60 ns for the carotenoid-containing WT, D1, D2, and T1 RCs, respectively (Figure S10, Table S1). A similar trend is also observed at 77 K with triplet energy transfer lifetime components of 75, 250, 116, and 290 ns for the WT, D1, D2, and T1 mutant RCs, respectively (Figure S11, Table S1). The increase in the timescale of triplet energy transfer (or the decrease of the rate) with decreasing temperature is more dramatic in the mutant RCs, particularly D1 and T1, than in WT.

The EADS with a lifetime of 1.4 μs at room temperature and 4.9−5.3 μs at 77 K observed for the carotenoid-containing RCs have the spectral characteristics of ^{3}Car. As expected, the decay time of ^{3}Car is the same for all samples and weakly dependent on temperature.[14]

For the carotenoid-less WT-NC and T1-NC RCs, only two EADS components corresponding to the decay of

DOI: 10.1021/acs.jpcb.8b07985
J. Phys. Chem. B 2018, 122, 10097−10107

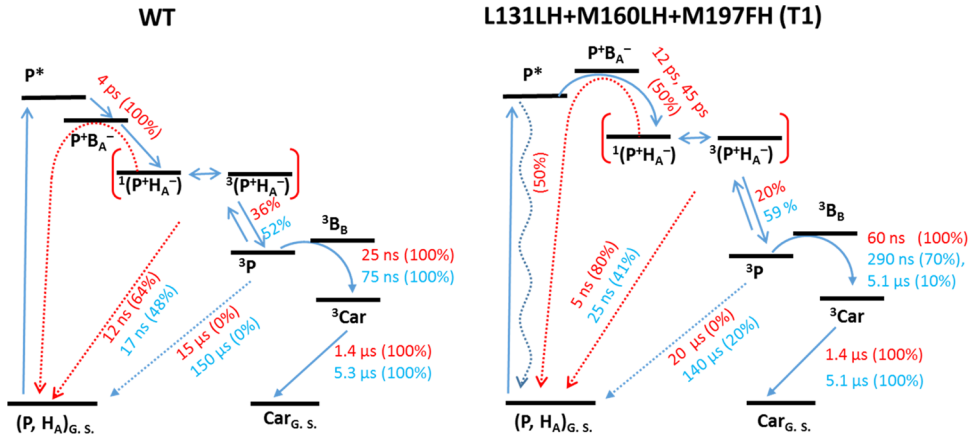

Figure 7. Kinetic scheme based on a dynamic heterogeneity model including time constants and yields of each reaction pathway at 298 K (red) and 77 K (light blue). This is based on global fitting analysis described in the Supporting Information and summarized in Table S1. The initial kinetic components and the yield of charge separation were obtained from fs-transient absorption data analysis (data not shown) and they are consistent with previous reports (refs 18, 19, and 40).

$^1(P^+H_A^-)/^3(P^+H_A^-)$ and the direct decay of ^3P to the ground state are obtained from the global fitting analysis (see Figure S12) of both the room-temperature and low-temperature data. As seen in Figure S12, the ^3P in these RCs decays directly to the ground state without triplet energy transfer in the range of 15−20 μs at room temperature and 110−150 μs at 77 K. At 77 K, the $^3P \rightarrow P$ decay is slightly faster in the T1-NC mutant (110 μs) than in the WT-NC mutant (150 μs). The difference in the decay time of ^3P between WT-NC and T1-NC mutant RCs without triplet energy transfer could be related to the decrease in ^3P energy in the hydrogen-bonded T1-NC mutant RCs (Figure S12). It was earlier pointed out by Robinson et al.[52] that triplet states lying relatively close to the ground singlet state decay more rapidly by the radiationless intersystem crossing process to the ground state. Boxer et al.[33] earlier reported that ^3P in the absence of triplet energy-transfer decays by intersystem crossing at low temperatures. However, at higher temperatures, an additional pathway can be activated through the reformation of the $^3(P^+H_A^-)$ followed by recombination that ultimately leads to the ground state of P.[33] The results also suggest that the $^3P \rightarrow P$ decay time is almost 2−3 orders of magnitude slower than the time for triplet energy transfer (Table S1).

It is worth mentioning that at room temperature the P bleaching amplitude in the 1.4 μs EADS of the carotenoid-containing RCs (representing the ^3P population) becomes almost zero (Figure S10) suggesting a near 100% efficiency of triplet energy transfer for all samples at room temperature. However, at low temperature (77 K), there are some P bleaching signals remaining in the 5 μs EADS of D1 RCs (almost 10−15% of the total ^3P population) and T1 RCs (almost 40−45% of the total ^3P population, Figure S11). In the D1 mutant, the residual ^3P decays with the decay time of ^3Car, whereas in the T1 mutant this residual ^3P population decays in part with the decay of ^3Car and the rest decays directly to the ground-state P without triplet energy transfer as evidenced by the 110 μs EADS of T1 at 77 K. The results suggest a pronounced kinetic heterogeneity associated to triplet energy transfer dynamics of the D1 and T1 mutants at low temperatures.

On the basis of this global fitting analysis, kinetic models are presented in Figure 7 that compare the overall dynamics and heterogeneity, including $^1(P^+H_A^-)/^3(P^+H_A^-)$ recombination, ^3P formation, and $^3P \rightarrow {}^3Car$ energy transfer between WT and the T1 mutant. The rates and yields of each reaction step are also summarized in Table S1 for all of the RC samples studied here.

3.5. Activation Energy Determination. From the analysis of the triplet energy-transfer rates at several different temperatures (in the range of 77−298 K), the activation energies were calculated for the WT and mutant RCs samples. Figure 8 shows the Arrhenius plots ($\ln k_{\text{triplet energy transfer}}$ vs $1/T$)

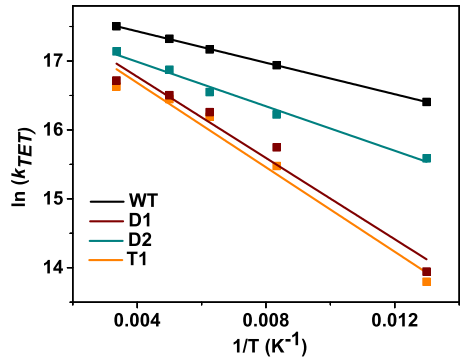

Figure 8. Arrhenius plot ($\ln(k_{TET})$ vs $1/T$) of the triplet energy transfer rate in quinone-depleted WT and mutant reaction centers. The activation energy values associated to the triplet energy transfer processes in different reaction centers were calculated from slope of the linear plot.

for all samples. The activation energy determined for the triplet energy transfer in WT RCs is around 80 cm^{-1}. Laible et al.[12] using time-resolved EPR measurements reported an activation energy of 105 cm^{-1} for WT RCs. An activation energy of 125 cm^{-1} was recently reported based on the transient absorption data analysis of WT, but in that study, the authors used only the longest time component resulting from a multiexponential fit of the triplet energy transfer kinetics at low temperature.[14] In contrast, in the current study, the average lifetime of the ^3P decay through triplet energy transfer was used to determine the activation energy. For the D1 and T1 mutants, the triplet energy transfer is kinetically heterogeneous at lower temperatures. A minor population of ^3P (around 10%) that decays slowly with the decay of ^3Car in 4.9−5.1 μs timescale (Figure

DOI: 10.1021/acs.jpcb.8b07985
J. Phys. Chem. B 2018, 122, 10097−10107

S11) was taken into account for averaging the lifetime of ^{3}P for the D1 and T1 mutants at those low temperatures. The calculated activation energies for the mutant RCs are 103, 204, and 213 cm^{-1} for D2, D1, and T1 mutant RCs, respectively. Considering the series from WT through T1, the activation energy increases by 133 cm^{-1}, whereas energy of the $^1(P^+H_A^-)/^3(P^+H_A^-)$ state increases by 260 meV as hydrogen bonds are added surrounding P in the mutant RCs.

3.6. Comparing Triplet Energy Transfer between WT and Mutants. The rate of triplet energy transfer is slower in the mutants compared to WT at both room and low temperatures (Figures S10 and S11, and Table S1). Past studies have concluded that the triplet energy-transfer rate is determined by an energetically unfavorable transfer of triplet energy from ^{3}P to ^3B_B, as evidenced previously by the dramatic slowing of this rate when B_B is replaced with a bacteriopheophytin.[14,29] The effect of mutations in the current study is most easily explained as a decrease in the energy of the ^{3}P state going from WT → D2 → D1 → T1. Stabilizing the energy of the ^{3}P state relative to the ground state would result in an increase in the energy difference between the ^{3}P and the ^3B_B states and hence decrease the rate of energy transfer. Among the double mutants, the ^{3}P energy is presumably stabilized more in D1 (L131LH + M160LH) than in D2 (L131LH + M197FH). The decrease of ^{3}P energy in the mutants compared to WT can be attributed to the influence of the environment of P on the electronic structure of its triplet state.[37]

The changes in the P/P$^+$ midpoint potentials resulting from the individual mutations are found to be additive in the multiple mutants.[53] If one assumes that the energy changes of the triplet states are also additive, then one would calculate changes of 9, 17, and 107 cm^{-1} in the activation energy of the triplet energy transfer due to the mutations at M197, L131, and M160, respectively. On the basis of this analysis, it appears that the mutation at the M160 position increases the activation energy to a greater extent than observed for the mutations at the M197 and L131 positions. Because the M160 mutation site is close to B_B, the mutation of Leu to His may alter the energy of the triplet state of B_B (^3B_B), as previously pointed out by Hoff and co-workers.[37] Thus, apart from the decrease of the ^{3}P energy, an increase in the energy of ^3B_B may also contribute for increasing the activation energy of the $^3P \rightarrow {}^3B_B \rightarrow$ Car triplet energy transfer for mutation at the M160 position.

Moreover, mutation-induced changes in the electronic spin distribution of the excited ^{3}P* state may influence the triplet energy-transfer rate by changing the electronic coupling. Richert et al. recently demonstrated the importance of electronic spin distribution symmetry in enhancing the triplet state delocalization in linear zinc porphyrin oligomers.[35] Several recent theoretical and experimental studies using the carotenoid-less mutant strain R26 of *R. sphaeroides* have demonstrated that the electronic spin density of P in its triplet excited state, ^{3}P*, is almost symmetrically distributed over the two moieties of P (P_L and P_M) with a minor charge-transfer character (slight excess in the L side).[54−56] The electronic spin density distributions of the triplet excited state of ^{3}P* in the mutant RCs are not known. Previously, from ENDOR studies of the WT and mutant RCs, it was suggested that for the radical cationic state of P (P$^{+\bullet}$), the mutations L131LH and M160LH each cause significant spin density shifts.[57] In the M160LH mutant RCs, the spin density distribution of the unpaired electron of P$^{+\bullet}$ is highly asymmetric with 85% of the spin density localized on P_L.[57] On the other hand, in the L131LH mutant RCs, the spin distribution of P$^{+\bullet}$ is localized more on P_M (53% localized on P_M).[57] In contrast, for the M197FH mutant RCs, the spin density distribution of the P$^{+\bullet}$ is very similar to that observed for the WT RCs (69% on P_L side).[57] From LD-ADMR study of the L131LH and M160LH mutant RCs of *R. sphaeroides*, Vrieze et al.[37] earlier pointed out that the change in the distribution of the unpaired electron in the triplet excited state (^{3}P*) qualitatively follows the same trend as the localization of spin density of the P$^{+\bullet}$ of the same mutant varies with respect to that of the WT RCs. Therefore, considering the large changes in the spin density distribution in the P of the M160LH and L131LH mutants relative to the WT, a large change in the rates of triplet energy transfer would be expected for the mutants, particularly M160LH containing mutants.

3.7. Singlet and Triplet Recombination Reaction Rates in Mutants. The $P^+H_A^-$ state includes contributions from both $^1(P^+H_A^-)$ and $^3(P^+H_A^-)$. The measurements described above provide insight into the relative rate constants for recombination of the singlet and triplet forms for $P^+H_A^-$. The decay of total population of $^1(P^+H_A^-)/^3(P^+H_A^-)$ can be represented by the following reaction kinetic scheme.[14]

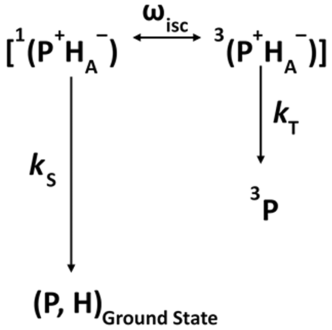

As reported earlier, the interconversion between the two virtually degenerate states, $^1(P^+H_A^-)$ and $^3(P^+H_A^-)$, has an oscillation frequency (ω_{isc}) in the range of 15 MH$_Z$ (a half-life period of 33 ns) for WT.[58] The oscillation process is relatively slow compared to the recombination reaction rates, k_S (1/19 ns^{-1} for WT) and k_T (1/(2−10) ns^{-1} for WT).[14] Therefore, the experimentally observed decay rate of the total population of $^1(P^+H_A^-)/^3(P^+H_A^-)$ can be approximated as the sum of two exponential decay rates, k_s and a rate limited by ω_{isc}. The time constants associated to these two individual decay steps can be estimated using the experimentally observed decay time (τ_{obs}) of the total population of $^1(P^+H_A^-)/^3(P^+H_A^-)$ (for example, 12 ns in WT, 10 ns in D1 and D2 mutants, and 5 ns in T1 mutant) and the yield of ^{3}P (Φ_T) (for example, 36% in WT, 28% in D1, 31% in D2, and 20% in the T1 mutant) using the following equation

$$\tau_{\text{recombination (S/T)}} = \tau_{obs}/\Phi_{\text{recombination (S/T)}}$$

where $\Phi_{\text{recombination}}$ (S/T) is the relative yield of the individual recombination reaction steps (singlet/triplet).[14,46] Thus, the estimated time constant for the singlet recombination reaction $^1(P^+H_A^-) \rightarrow (P, H)_{g.s}$ is found to be decreased from 19 ns in WT, to 14 ns in D1 and D2 mutants, and 6 ns in T1 mutant (see Table S1) at room temperature. The above calculation also provided the time constant for the overall process of triplet conversion $^1(P^+H_A^-) \leftrightarrow {}^3(P^+H_A^-) \rightarrow {}^3$P. In the WT RC, the estimated time constant for this process is 33 ns, which

DOI: 10.1021/acs.jpcb.8b07985
J. Phys. Chem. B 2018, 122, 10097−10107

correlates well to the half-life period of $^1(P^+H_A^-) \leftrightarrow {}^3(P^+H_A^-)$ oscillation.[58] This time constant is similar for the double (33 ns) and triple mutant (25 ns) RCs.

4. CONCLUSIONS

The rate of triplet energy transfer between ^3P and the carotenoid decreases in L131LH + M160LH (D1), L131LH + M197FH (D2), and L131LH + M160LH + M197FH (T1) mutants with additional hydrogen bonds to P. This is consistent with a decrease in the energy of ^3P in the mutants that increases the energy gap between ^3P and the bridging ^3B_B state, making it thermally less accessible. As the temperature decreases from 298 to 77 K, the triplet energy transfer time increases (i.e., rate decreases) dramatically in the D1 and T1 mutants, consistent with an increase of activation energy for this process in the mutants relative to the WT. The increase of the activation energy is 133 cm^{-1} for the T1 mutant relative to the WT RCs due to the stabilization of ^3P energy. The extent of these energetic changes is small compared to the much larger destabilization (by almost 260 meV) of the energy of $P^+H_A^-$ state of the mutant associated to the changes of the P/P^+ midpoint potential. In addition to these energetic considerations, the rate changes can also be attributed to the significant changes in the spin density distribution of the bacteriochlorophylls of P induced by the mutation, which also could lead to slower triplet energy-transfer processes.

■ ASSOCIATED CONTENT

Supporting Information

The Supporting Information is available free of charge on the ACS Publications website at DOI: 10.1021/acs.jpcb.8b07985.

Ground-state absorption spectra of all RC samples; two-dimensional contour plots of transient absorption spectra of D1 and D2 mutant RCs; the time-resolved absorption spectra and the EADS spectra of different RCs (PDF)

■ AUTHOR INFORMATION

Corresponding Authors

*E-mail: smandal@nitt.edu (S.M.).
*E-mail: nwoodbury@asu.edu (N.W.W.).

ORCID

Sarthak Mandal: 0000-0002-5592-9664
James P. Allen: 0000-0002-7760-3921

Present Address

§Department of Chemistry, National Institute of Technology, Tiruchirappalli, Tamil Nadu 620015, India

Notes

The authors declare no competing financial interest.

■ ACKNOWLEDGMENTS

This work was funded by NSF grants MCB-1157788 and CHE-1505874.

■ REFERENCES

(1) Kromdijk, J.; Glowacka, K.; Leonelli, L.; Gabilly, S. T.; Iwai, M.; Niyogi, K. K.; Long, S. P. Improving Photosynthesis and Crop Productivity by Accelerating Recovery from Photoprotection. *Science* **2016**, *354*, 857−861.

(2) Staleva, H.; Komenda, J.; Shukla, M. K.; Slouf, V.; Kana, R.; Polivka, T.; Sobotka, R. Mechanism of Photoprotection in the Cyanobacterial Ancestor of Plant Antenna Proteins. *Nat. Chem. Biol.* **2015**, *11*, 287−291.

(3) Bode, S.; Quentmeier, C. C.; Liao, P. N.; Hafi, N.; Barros, T.; Wilk, L.; Bittner, F.; Walla, P. J. On the Regulation of Photosynthesis by Excitonic Interactions between Carotenoids and Chlorophylls. *Proc. Natl. Acad. Sci. U.S.A.* **2009**, *106*, 12311−12316.

(4) Holt, N. E.; Zigmantas, D.; Valkunas, L.; Li, X. P.; Niyogi, K. K.; Fleming, G. R. Carotenoid Cation Formation and the Regulation of Photosynthetic Light Harvesting. *Science* **2005**, *307*, 433−436.

(5) Kirilovsky, D. Dissipating Energy by Carotenoids. *Nat. Chem. Biol.* **2015**, *11*, 242−243.

(6) Ruban, A. V.; Berera, R.; Ilioaia, C.; van Stokkum, I. H. M.; Kennis, J. T. M.; Pascal, A. A.; van Amerongen, H.; Robert, B.; Horton, P.; van Grondelle, R. Identification of a Mechanism of Photoprotective Energy Dissipation in Higher Plants. *Nature* **2007**, *450*, 575−578.

(7) Fraser, N. J.; Hashimoto, H.; Cogdell, R. J. Carotenoids and Bacterial Photosynthesis: The Story So Far. *Photosynth. Res.* **2001**, *70*, 249−256.

(8) Chidsey, C. E. D.; Kirmaier, C.; Holten, D.; Boxer, S. G. Magnetic-Field Dependence of Radical-Pair Decay Kinetics and Molecular Triplet Quantum Yield in Quinone-Depleted Reaction Centers. *Biochim. Biophys. Acta, Bioenerg.* **1984**, *766*, 424−437.

(9) Cogdell, R. J.; Monger, T. G.; Parson, W. W. Carotenoid Triplet-States in Reaction Centers from *Rhodopseudomonas sphaeroides* and *Rhodospirillum rubrum*. *Biochim. Biophys. Acta, Bioenerg.* **1975**, *408*, 189−199.

(10) Frank, H. A.; Chynwat, V.; Posteraro, A.; Hartwich, G.; Simonin, I.; Scheer, H. Triplet State Energy Transfer between the Primary Donor and the Carotenoid in *Rhodobacter sphaeroides* R-26.1 Reaction Centers Exchanged with Modified Bacteriochlorophyll Pigments and Reconstituted with Spheroidene. *Photochem. Photobiol.* **1996**, *64*, 823−831.

(11) Hartwich, G.; Scheer, H.; Aust, V.; Angerhofer, A. Absorption and Admr Studies on Bacterial Photosynthetic Reaction Centers with Modified Pigments. *Biochim. Biophys. Acta, Bioenerg.* **1995**, *1230*, 97−113.

(12) Laible, P. D.; Morris, Z. S.; Thurnauer, M. C.; Schiffer, M.; Hanson, D. K. Inter- and Intraspecific Variation in Excited-State Triplet Energy Transfer Rates in Reaction Centers of Photosynthetic Bacteria. *Photochem. Photobiol.* **2003**, *78*, 114−123.

(13) Ullrich, J.; Speer, R.; Greis, J.; Vonschutz, J. U.; Wolf, H. C.; Cogdell, Richard Carotenoid Triplet-States in Pigment Protein Complexes from Photosynthetic Bacteria - Absorption-Detected Magnetic-Resonance from 4 to 225 K. *Chem. Phys. Lett.* **1989**, *155*, 363−370.

(14) Mandal, S.; Carey, A. M.; Locsin, J.; Gao, B. R.; Williams, J. C.; Allen, J. P.; Lin, S.; Woodbury, N. W. Mechanism of Triplet Energy Transfer in Photosynthetic Bacterial Reaction Centers. *J. Phys. Chem. B* **2017**, *121*, 6499−6510.

(15) Allen, J. P.; Feher, G.; Yeates, T. O.; Komiya, H.; Rees, D. C. Structure of the Reaction Center from *Rhodobacter sphaeroides* R-26: The Cofactors. *Proc. Natl. Acad. Sci. U.S.A.* **1987**, *84*, 5730−5734.

(16) Steffen, M. A.; Lao, K.; Boxer, S. G. Dielectric Asymmetry in the Photosynthetic Reaction Center. *Science* **1994**, *264*, 810−816.

(17) Yanagi, K.; Shimizu, M.; Hashimoto, H.; Gardiner, A. T.; Roszak, A. W.; Cogdell, R. J. Local Electrostatic Field Induced by the Carotenoid Bound to the Reaction Center of the Purple Photosynthetic Bacterium *Rhodobacter sphaeroides*. *J. Phys. Chem. B* **2005**, *109*, 992−998.

(18) Pan, J.; Saer, R. G.; Lin, S.; Guo, Z.; Beatty, J. T.; Woodbury, N. W. The Protein Environment of the Bacteriopheophytin Anion Modulates Charge Separation and Charge Recombination in Bacterial Reaction Centers. *J. Phys. Chem. B* **2013**, *117*, 7179−7189.

(19) Wang, H.; Hao, Y.; Jiang, Y.; Lin, S.; Woodbury, N. W. Role of Protein Dynamics in Guiding Electron-Transfer Pathways in Reaction Centers from *Rhodobacter sphaeroides*. *J. Phys. Chem. B* **2012**, *116*, 711−717.

DOI: 10.1021/acs.jpcb.8b07985
J. Phys. Chem. B 2018, 122, 10097−10107

(20) Woodbury, N. W.; Allen, J. P., The Pathway, Kinetics and Thermodynamics of Electron Transfer in Wild Type and Mutant Reaction Centers of Purple Nonsulfur Bacteria. In *Anoxygenic Photosynthetic Bacteria*; Blankenship, R. E.; Madigan, M. T.; Bauer, C. E., Eds.; Springer: Netherlands, 1995; pp 527−557.
(21) Haberkorn, R.; Michelbeyerle, M. E. Mechanism of Triplet Formation in Photosynthesis Via Hyperfine Interaction. *FEBS Lett.* **1977**, *75*, 5−8.
(22) Schenck, C. C.; Blankenship, R. E.; Parson, W. W. Radical-Pair Decay Kinetics, Triplet Yields and Delayed Fluorescence from Bacterial Reaction Centers. *Biochim. Biophys. Acta, Bioenerg.* **1982**, *680*, 44−59.
(23) Schenck, C. C.; Mathis, P.; Lutz, M. Triplet Formation and Triplet Decay in Reaction Centers from the Photosynthetic Bacterium *Rhodopseudomonas sphaeroides*. *Photochem. Photobiol.* **1984**, *39*, 407−417.
(24) Farhoosh, R.; Chynwat, V.; Gebhard, R.; Lugtenburg, J.; Frank, H. A. Triplet Energy Transfer between the Primary Donor and Carotenoids in *Rhodobacter sphaeroides* R-26.1 Reaction Centers Incorporated with Spheroidene Analogs Having Different Extents of Pi-Electron Conjugation. *Photochem. Photobiol.* **1997**, *66*, 97−104.
(25) Angerhofer, A.; Bornhauser, F.; Aust, V.; Hartwich, G.; Scheer, H. Triplet Energy Transfer in Bacterial Photosynthetic Reaction Centres. *Biochim. Biophys. Acta, Bioenerg.* **1998**, *1365*, 404−420.
(26) Jordanides, X. J.; Scholes, G. D.; Fleming, G. R. The Mechanism of Energy Transfer in the Bacterial Photosynthetic Reaction Center. *J. Phys. Chem. B* **2001**, *105*, 1652−1669.
(27) You, Z. Q.; Hsu, C. P.; Fleming, G. R. Triplet-Triplet Energy-Transfer Coupling: Theory and Calculation. *J. Chem. Phys.* **2006**, *124*, No. 044506.
(28) Aust, V.; Angerhofer, A.; Ullrich, J.; Vonschutz, J. U.; Wolf, H. C.; Cogdell, R. J. Admr of Carotenoid Triplet-States in Bacterial Photosynthetic Antenna and Reaction Center Complexes. *Chem. Phys. Lett.* **1991**, *181*, 213−221.
(29) deWinter, A.; Boxer, S. G. The Mechanism of Triplet Energy Transfer from the Special Pair to the Carotenoid in Bacterial Photosynthetic Reaction Centers. *J. Phys. Chem. B* **1999**, *103*, 8786−8789.
(30) Frank, H. A.; Violette, C. A. Monomeric Bacteriochlorophyll Is Required for the Triplet Energy-Transfer between the Primary Donor and the Carotenoid in Photosynthetic Bacterial Reaction Centers. *Biochim. Biophys. Acta* **1989**, *976*, 222−232.
(31) Arellano, J. B.; Melo, T. B.; Fyfe, P. K.; Cogdell, R. J.; Naqvi, K. R. Multichannel Flash Spectroscopy of the Reaction Centers of Wild-Type and Mutant *Rhodobacter sphaeroides*: Bacteriochlorophll(B)-Mediated Interaction between the Carotenoid Triplet and the Special Pair. *Photochem. Photobiol.* **2004**, *79*, 68−75.
(32) Marchanka, A.; Paddock, M.; Lubitz, W.; van Gastel, M. Low-Temperature Pulsed Epr Study at 34 Ghz of the Triplet States of the Primary Electron Donor P-865 and the Carotenoid in Native and Mutant Bacterial Reaction Centers of *Rhodobacter sphaeroides*. *Biochemistry* **2007**, *46*, 14782−14794.
(33) de Winter, A.; Boxer, S. G. Energetics of Primary Charge Separation in Bacterial Photosynthetic Reaction Center Mutants: Triplet Decay in Large Magnetic Fields. *J. Phys. Chem. A* **2003**, *107*, 3341−3350.
(34) Rautter, J.; Lendzian, F.; Lubitz, W.; Wang, S.; Allen, J. P. Comparative Study of Reaction Centers from Photosynthetic Purple Bacteria: Electron Paramagnetic Resonance and Electron Nuclear Double Resonance Spectroscopy. *Biochemistry* **1994**, *33*, 12077−12084.
(35) Richert, S.; Bullard, G.; Rawson, J.; Angiolillo, P. J.; Therien, M. J.; Timmel, C. R. On the Importance of Electronic Symmetry for Triplet State Delocalization. *J. Am. Chem. Soc.* **2017**, *139*, 5301−5304.
(36) Artz, K.; Williams, J. C.; Allen, J. P.; Lendzian, F.; Rautter, J.; Lubitz, W. Relationship between the Oxidation Potential and Electron Spin Density of the Primary Electron Donor in Reaction Centers from *Rhodobacter sphaeroides*. *Proc. Natl. Acad. Sci. U.S.A.* **1997**, *94*, 13582−13587.
(37) Vrieze, J.; Williams, J. C.; Allen, J. P.; Hoff, A. J. An Ld-Admr Study on Reaction Centers of the Lh(L131) and Lh(M160) Hydrogen-Bonding Mutants of *Rhodobacter sphaeroides*. *Biochim. Biophys. Acta, Bioenerg.* **1996**, *1276*, 221−228.
(38) Lin, X.; Murchison, H. A.; Nagarajan, V.; Parson, W. W.; Allen, J. P.; Williams, J. C. Specific Alteration of the Oxidation Potential of the Electron-Donor in Reaction Centers from Rhodobacter-Sphaeroides. *Proc. Natl. Acad. Sci. U.S.A.* **1994**, *91*, 10265−10269.
(39) Ortega, J. M.; Mathis, P.; Williams, J. C.; Allen, J. P. Temperature Dependence of the Reorganization Energy for Charge Recombination in the Reaction Center from *Rhodobacter sphaeroides*. *Biochemistry* **1996**, *35*, 3354−3361.
(40) Woodbury, N. W.; Lin, S.; Lin, X. M.; Peloquin, J. M.; Taguchi, A. K. W.; Williams, J. C.; Allen, J. P. The Role of Reaction-Center Excited-State Evolution During Charge Separation in a Rhodobacter-Sphaeroides Mutant with an Initial Electron-Donor Midpoint Potential 260 Mv above Wild-Type. *Chem. Phys.* **1995**, *197*, 405−421.
(41) Kanchanawong, P.; Dahlbom, M. G.; Treynor, T. P.; Reimers, J. R.; Hush, N. S.; Boxer, S. G. Charge Delocalization in the Special-Pair Radical Cation of Mutant Reaction Centers of *Rhodobacter sphaeroides* from Stark Spectra and Nonadiabatic Spectral Simulations. *J. Phys. Chem. B* **2006**, *110*, 18688−18702.
(42) Moore, L. J.; Zhou, H. L.; Boxer, S. G. Excited-State Electronic Asymmetry of the Special Pair in Photosynthetic Reaction Center Mutants: Absorption and Stark Spectroscopy. *Biochemistry* **1999**, *38*, 11949−11960.
(43) Reimers, J. R.; Hush, N. S. Unified Description of the Electrochemical, Charge Distribution, and Spectroscopic Properties of the Special-Pair Radical Cation in Bacterial Photosynthesis. *J. Am. Chem. Soc.* **2004**, *126*, 4132−4144.
(44) Ridge, J. P.; van Brederode, M. E.; Goodwin, M. G.; van Grondelle, R.; Jones, M. R. Mutations That Modify or Exclude Binding of the Qa Ubiquinone and Carotenoid in the Reaction Center from *Rhodobacter sphaeroides*. *Photosynth. Res.* **1999**, *59*, 9−26.
(45) Okamura, M. Y.; Isaacson, R. A.; Feher, G. Primary Acceptor in Bacterial Photosynthesis - Obligatory Role of Ubiquinone in Photoactive Reaction Centers of Rhodopseudomonas-Spheroides. *Proc. Natl. Acad. Sci. U.S.A.* **1975**, *72*, 3491−3495.
(46) Sun, C.; Carey, A. M.; Gao, B. R.; Wraight, C. A.; Woodbury, N. W.; Lin, S. Ultrafast Electron Transfer Kinetics in the Lm Dimer of Bacterial Photosynthetic Reaction Center from *Rhodobacter sphaeroides*. *J. Phys. Chem. B* **2016**, *120*, 5395−5404.
(47) Gibasiewicz, K.; Bialek, R.; Pajzderska, M.; Karolczak, J.; Burdzinski, G.; Jones, M. R.; Brettel, K. Weak Temperature Dependence of $P^+ H_A^-$ Recombination in Mutant *Rhodobacter sphaeroides* Reaction Centers. *Photosynth. Res.* **2016**, *128*, 243−258.
(48) Gibasiewicz, K.; Pajzderska, M.; Dobek, A.; Karolczak, J.; Burdzinski, G.; Brettel, K.; Jones, M. R. Analysis of the Temperature-Dependence of P^+H^{A-} Charge Recombination in the *Rhodobacter sphaeroides* Reaction Center Suggests Nanosecond Temperature-Independent Protein Relaxation. *Phys. Chem. Chem. Phys.* **2013**, *15*, 16321−16333.
(49) Pan, J.; Saer, R.; Lin, S.; Beatty, J. T.; Woodbury, N. W. Electron Transfer in Bacterial Reaction Centers with the Photoactive Bacteriopheophytin Replaced by a Bacteriochlorophyll through Coordinating Ligand Substitution. *Biochemistry* **2016**, *55*, 4909−4918.
(50) Nagarajan, V.; Parson, W. W.; Gaul, D.; Schenck, C. Effect of Specific Mutations of Tyrosine-(M)210 on the Primary Photosynthetic Electron-Transfer Process in Rhodobacter-Sphaeroides. *Proc. Natl. Acad. Sci. U.S.A.* **1990**, *87*, 7888−7892.
(51) Tang, C. K.; Williams, J. A. C.; Taguchi, A. K. W.; Allen, J. P.; Woodbury, N. W. P + Ha- Charge Recombination Reaction Rate Constant in *Rhodobacter sphaeroides* Reaction Centers Is Independent of the P/P + Midpoint Potential. *Biochemistry* **1999**, *38*, 8794−8799.
(52) Robinson, G. W. Dynamic Role of Triplet States in Photosynthesis. *Proc. Natl. Acad. Sci. U.S.A.* **1963**, *49*, 521−529.
(53) Müh, F.; Lendzian, F.; Roy, M.; Williams, J. C.; Allen, J. P.; Lubitz, W. Pigment-Protein Interactions in Bacterial Reaction Centers and Their Influence on Oxidation Potential and Spin Density

DOI: 10.1021/acs.jpcb.8b07985
J. Phys. Chem. B 2018, 122, 10097−10107

Distribution of the Primary Donor. *J. Phys. Chem. B* **2002**, *106*, 3226−3236.
(54) Norris, J. R.; Budil, D. E.; Gast, P.; Chang, C. H.; Elkabbani, O.; Schiffer, M. Correlation of Paramagnetic States and Molecular-Structure in Bacterial Photosynthetic Reaction Centers - the Symmetry of the Primary Electron-Donor in *Rhodopseudomonas viridis* and *Rhodobacter sphaeroides* R-26. *Proc. Natl. Acad. Sci. U. S. A.* **1989**, *86*, 4335−4339.
(55) Thamarath, S. S.; Bode, B. E.; Prakash, S.; Gupta, K. B. S. S.; Alia, A.; Jeschke, G.; Matysik, J. Electron Spin Density Distribution in the Special Pair Triplet of *Rhodobacter sphaeroides* R26 Revealed by Magnetic Field Dependence of the Solid-State Photo-Cidnp Effect. *J. Am. Chem. Soc.* **2012**, *134*, 5921−5930.
(56) Kobori, Y.; Ponomarenko, N.; Norris, J. R. Time-Resolved Electron Paramagnetic Resonance Study on Cofactor Geometries and Electronic Couplings after Primary Charge Separations in the Photosynthetic Reaction Center. *J. Phys. Chem. C* **2015**, *119*, 8078−8088.
(57) Rautter, J.; Lendzian, F.; Schulz, C.; Fetsch, A.; Kuhn, M.; Lin, X.; Williams, J. C.; Allen, J. P.; Lubitz, W. Endor Studies of the Primary Donor Cation-Radical in Mutant Reaction Centers of *Rhodobacter sphaeroides* with Altered Hydrogen-Bond Interactions. *Biochemistry* **1995**, *34*, 8130−8143.
(58) Bittl, R.; Vanderest, A.; Kamlowski, A.; Lubitz, W.; Stehlik, D. Time-Resolved Epr of the Radical Pair P(865)(+)Q(a)(-) in Bacterial Reaction Centers - Observation of Transient Nutations, Quantum Beats and Envelope Modulation Effects. *Chem. Phys. Lett.* **1994**, *226*, 349−358.

DOI: 10.1021/acs.jpcb.8b07985
J. Phys. Chem. B 2018, 122, 10097−10107